UNIVERSITY OF LEEDS

This is a repository copy of *Rationalising mAb candidate screening using a single holistic developability parameter*.

White Rose Research Online URL for this paper:
https://eprints.whiterose.ac.uk/220534/

Version: Accepted Version

Article:

White Rose
university consortium
Universities of Leeds, Sheffield & York

eprints@whiterose.ac.uk
https://eprints.whiterose.ac.uk/

1 **Rationalising mAb candidate screening using a single holistic**

2 **developability parameter**

3 Leon F. Willis[a,b], Isabelle Trayton[c], Janet C. Saunders[c], Maria G. Brùque[c#],

4 William Davis Birch[d], David R. Westhead[a], Katie Day[c], Nicholas J. Bond[c], Paul

5 W.A. Devine[c], Christopher Lloyd[c], Nikil Kapur[d], Sheena E. Radford[a,b],

6 Nicholas J. Darton[c*] and David J. Brockwell[a,b*]

7 *[a] School of Molecular and Cellular Biology, Faculty of Biological Sciences, University of*

8 *Leeds, Leeds, UK; [b] Astbury Centre for Structural Molecular Biology, University of Leeds,*

9 *Leeds, UK; [c]AstraZeneca, The Discovery Centre, Cambridge, UK; [d] School of Mechanical*

10 *Engineering, Faculty of Engineering and Physical Sciences, University of Leeds, Leeds, UK;*

11 *[#] Present Address: EPSRC Centre for Doctoral Training in Formulation Engineering,*

12 *University of Birmingham, Birmingham, UK*

13 Correspondence to Nicholas J. Darton[*] (nicholas.darton@astrazeneca.com) or David J.

14 Brockwell[*] (D.J.Brockwell@leeds.ac.uk)

15

16

17

18

19

20

21

22

23

24

25

26

27

28

29

Abstract

A framework for the rational selection of a minimal suite of non-degenerate developability assays (DAs) that maximise insight into candidate developability or storage stability is lacking. To address this, we subjected nine formulation:mAbs to twelve mechanistically distinct DAs together with measurement of their accelerated and long-term storage stability. We show that it is possible to identify a reduced set of key variables from this suite of DAs using orthogonal statistical methods. We exemplify our approach by predicting the rank formulation:mAb degradation rate at 25 °C (determined over six months) using just five DAs that can be measured in less than a day, spanning a range of physicochemical features. Implementing such approaches focuses resources, thus increasing sustainability and decreasing development costs.

Introduction

The adoption of the Quality by Design paradigm by the biopharmaceutical industry over the past two decades[1] has led to the emergence of the concept of "developability". This can be broadly defined as the selection of molecules with desirable biochemical and biophysical attributes, which increase the chances of translation to a commercial therapeutic manufactured at large scale.[2–4] Focussing on monoclonal antibodies (mAbs), many biophysical assays have been employed to probe different physicochemical characteristics of these proteins, including: solubility;[5–7] liabilities in the complementarity determining regions (CDRs);[8] susceptibility to thermal stress;[9,10] undesired interfacial adsorption[11–13] and aggregation propensity.[14–18] Since the seminal work of Jain et al.,[4] many groups have used Pearson[7] or Spearman's rank correlation[12,19] to relate the behaviour of molecules in different assays and examine the

2

55   relationships between different *in vitro* and *in silico* methods.[20–23] Nevertheless, a framework

56   to link the outputs of these developability assessments to a chosen measurable attribute of

57   manufacturability is lacking. Ability to do this would decrease the time for development, de-

58   risk candidate selection and scale-up, and increase sustainability, bringing enhanced provision

59   of medicines to patients.

60   To address this issue, here we describe a logical framework to condense the outputs of a

61   focussed set of Developability Assays (DAs) to a single parameter. This parameter, derived

62   from assays employed early in development, has predictive power of a user-defined measurable

63   attribute of manufacturability (Figure 1). To do this we obtain a dataset derived from twelve

64   mechanistically distinct DAs (with the outputs captured by 23 variables) including *in silico*

65   analyses on three IgG1s in three formulations and complement these with long-term and

66   accelerated stability data obtained in the same buffers (captured by nine variables). As

67   accelerated and long-term (i.e. real-time) degradation rates are universal, yet expensive-to-

68   determine quality attributes essential within the regulatory framework (for a typical mAb, this

69   takes over two years and consumes grams of material)[24] we chose the kinetic stability of the

70   samples at 25 °C as our measurable attribute of manufacturability.

71   Statistical analysis of the dataset shows that the DAs are grouped into four families that probe

72   distinct biophysical features which can be used to rank formulation:mAbs holistically. We

73   then show that a combination of suitably scaled outputs from a focussed, non-degenerate set of

74   DAs that probe multiple biophysical attributes can be used as an indicator of kinetic stability

75   early in the development pipeline by predicting relative storage stability at 25 °C. The general

76   methodology (which could be applied to other manufacturing attributes of the user's choosing),

77   is rapid and resource-efficient and its ability to capture storage stability, de-risks and increases

78   the sustainability of early-stage candidate selection.

3
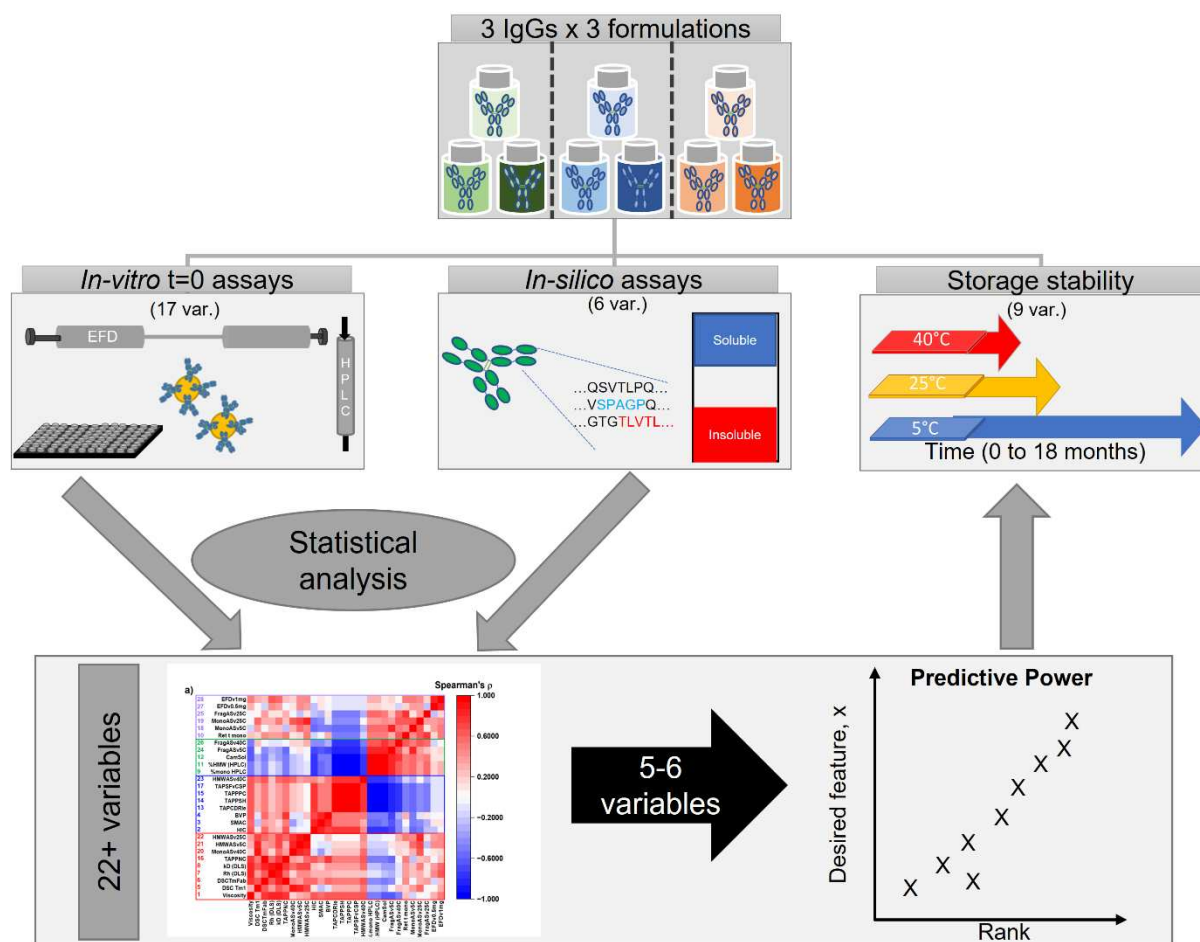
Figure 1. Overview of the study. Three IgG1s were placed in three different buffer conditions (histidine-arginine (green, buffer A), histidine-sucrose (blue, buffer B) and sodium citrate (brown, buffer C)), to yield nine formulation:mAb pairs. Each sample was analysed with ten *in-vitro* developability assays (including the Extensional Flow Device (EFD)) and two *in-silico* analyses, followed by accelerated and long-term storage stability over three to eighteen months. The completed dataset (comprising at least 600 measurements) was analysed and condensed to 32 reported assay variables, per sample. The dataset was then scrutinised with an array of statistical tools. As a proof of concept, we examine whether our framework can predict the rank order of the kinetic stability of our samples at 25 °C, which is resource-intensive in terms of both time and material, using less resource-intensive "time equal zero" assays.

Experimental Section

2.1 Antibodies and formulations

All antibodies were expressed in an IgG1 format in CHO cells and purified from the culture medium using Protein A chromatography.[25] Each IgG1 (mAb1, mAb2 and mAb3) was then dialysed into the following formulations: 20 mM L-His, 190 mM L-arginine, pH 6 (formulation A); 20 mM L-His, 220 mM (7.5% w/v) sucrose, pH 6 (formulation B) and 25 mM sodium citrate, pH 5.0 (formulation C) by repetitive buffer exchanges using Millipore Centricon 30,000 MWCO filters, according to the manufacturer's protocol. Briefly, the tubes were primed with 15 mL of the new formulation buffer and centrifuged at 3500 $\times g$ for 10 mins. The sample was loaded into the tubes and centrifuged as before for 30 mins. The filtrate was discarded and the retentate diluted to 15 mL with formulation buffer. This process was repeated at least 5 more times, until the final desired concentration and volume was reached.

Protein concentration was determined at 280 nm using a Trinean DropSense96 UV-Vis spectrophotometer. Samples were diluted to a final concentration of 50 mg/mL, then syringe-filtered through a 0.22 µm filter (Millipore) in a laminar flow hood. 10% (w/v) PS80 was added to each mAb/formulation to a final concentration of 0.02% (w/v) and then re-filtered under sterile conditions (0.22 µm), then vialed in 1.1 mL aliquots using 2R glass vials, rubber stoppers and crimp sealed. One set of vials was frozen at -80 ˚C, for use later in HIC, SMAC and EFD assays. The osmolality and pH of the samples were measured using an OsmoPro and Mettler Toledo pH meter, respectively, to confirm the formulations were within specification (see Supplementary Information).

For reference, this yields three IgGs in three formulations (nine samples in total), with the code names displayed in the unshaded boxes in Table 1.

Formulation:mAb	mAb1	mAb2	mAb3
Formulation A (His-Arg)	A1	A2	A3
Formulation B (His-sucrose)	B1	B2	B3
Formulation C (Na citrate)	C1	C2	C3

119   **Table 1**. Nomenclature for IgGs and buffer conditions used.

120

121   **2.2 Developability assays**

122   Methods for the rheology of (surfactant-free) formulations, HIC, SMAC, BVP-ELISA, AC-

123   SINS, DSC, DLS, BMI, CamSol, TAP and soluble protein concentration measurements are

124   provided in the Supplementary Methods.

125

126   **2.3 Extensional Flow Device (EFD) and HPLC assay**

127   Design and operation details of the EFD can be found elsewhere.[16,26–28] The current work used

128   a modified version the original device, with a 3D-printed insert allowing three pairs of 1 mL

129   Gastight Hamilton syringes to be mounted and driven simultaneously. Each EFD experiment

130   initially begins with 3 × buffer-rinsed syringes fitted with fresh 75 mm long, 0.3 mm i.d.

131   borosilicate glass capillaries (Sutter Instruments) *via* ferrule compression fittings (Hamilton)

132   and Gilson P10 O-rings. The mAb solutions were prepared from thawed vials of each

133   respective formulation. The aliquot was diluted ~10 fold in its respective formulation buffer,

134   syringe-filtered (0.22 µm, Millipore) and the concentration determined (after a further 20-fold

135   dilution) by UV-Vis spectroscopy (Shimadzu UV-1800). 0.5 mL of protein solution (0.25-,

136   0.5- and 1 mg/mL) was drawn into each respective sample syringe, removing visible air

137   bubbles prior to connection to their buffer-rinsed "receiver" syringe. The syringe pairs were

138   fixed with top-mounted 3D-printed clamps, before being driven by a linear stage using a

139   stepper motor at velocity of 8 mm/s for a defined number of passes (10–500). The pass

6

140   conditions were controlled by a microprocessor and visual display. Once finished, syringes

141   were disassembled, the solutions slowly placed into fresh Eppendorf tubes and kept on ice.

142   Control samples were incubated ambiently alongside the 500 passes samples (which takes ~

143   50 mins to complete) at each concentration. The syringes were washed with 2% (v/v)

144   Hellmanex-III (aq), Milli-Q water and formulation buffer prior to each new experiment.

145   To quantify EFD-induced aggregation, samples were clarified by ultracentrifugation, spinning

146   2×150 µL of each sample for 30 mins at 30,000 rpm (TLA100 rotor, Beckmann Coulter). 2

147     $\times$ 100 µL supernatant was removed from each respective sample tube, with the supernatants

148   then combined and loaded in a 300 µL conical insert polypropylene vial (VWR), before crimp-

149   sealing with PTFE/Aluminum lids (ThermoFisher). Samples were analysed by HP-SEC on a

150   Shimadzu Nexera LC-40 system. 20 µL of sample was injected onto a TOSOH G3000swxl

151   column, eluting isocratically with HP-SEC mobile phase (0.1 M sodium phosphate dibasic, 0.1

152   M sodium sulfate pH 6.8), at a flow rate of 0.5 mL/min. Following detection at 280 nm with a

153   PDA detector, the chromatograms were integrated in LabSolutions software, and % monomer

154   remaining calculated by normalising the peak areas to those of the respective, quiescent control

155   samples. The observed rate of monomer loss was computed using the SLOPE function in

156   Microsoft Excel.

157

158   **2.4 Accelerated (AS) and long-term storage stability study**

159   This study commenced in January 2020. Boxes containing vials of A1–C3 were placed in

160   incubators at the temperatures and for the durations stated in Table 2:

161

162

163

Incubator Temperature	t=0	Timepoint 1 (months)	Timepoint 2 (months)	Timepoint 3 (months)	Timepoint 4 (months)
40 °C	t=0	0.5	1	3	-
25 °C	t=0	1	3	6	-
5 °C	t=0	3	6	12	18

164 **Table 2**: List of samples taken for analysis form the stability study.

165 Due to the COVID-19 pandemic, all timepoint samples (apart from 0-, 0.5- and 1-month

166 samples) were pooled and stored at -80 °C prior to their quantification in April 2022. To

167 quantify the species remaining in solution at each timepoint, samples were diluted 1:4 in PBS

168 (Sigma) into a 0.45-µm centrifugal filter unit (Millipore) and spun at 16,700 $\times g$ for 1 minute.

169 Alongside the formulated samples, a series of standards (PBS, HP-SEC mobile phase (0.1 M

170 sodium phosphate dibasic, 0.1 M sodium sulfate pH 6.8), Nip228 reference standard IgG (in

171 20 mM L-His, 240 mM sucrose pH 6.0) and BioRad column calibrants) were clarified in the

172 same fashion.

173 2×25 µL of sample was injected onto a TOSOH G3000swxl column, equipped with a guard

174 column. The samples were eluted isocratically in the HP-SEC mobile phase at 1 mL/min on an

175 Agilent HPLC system. Peak areas were quantified by integration using ChemStation software.

176 The monomer peak was considered as the major peak with a retention time ~8.3 min. Any

177 peaks detected with a shorter retention are higher molecular weight species (HMW). Any peaks

178 that elute after the monomer are considered fragments. The area values were input into Excel,

179 including the standards, which all passed internal validation levels. After averaging the

180 technical replicates, the SLOPE function was used to determine the observed relative rates of

181 % change in monomer, HMW content and % fragment over the respective time courses above.

182 We thus highlight that all the observed rates pertaining to the kinetic stability study are relative

183 observed rates, but we omit "relative" for brevity throughout the manuscript.

184   Finally, the error on the observed rate of change in % monomer at 25 °C test dataset was

185   calculated by including the error (s.d.) from both technical replicates for each formulation. The

186   average coefficient of variation from the SLOPE analysis (for the entire dataset =

187   0.036%/month) was used as a default value where samples had zero error. Instrumental error

188   weighting was used ($1/CV^2$) and a linear fit ($y = a + bx$) performed in OriginPro to obtain the

189   gradient (b) and standard error (from the fit) for each formulation (Figure 3).   This analysis

190   was also performed on the 5°C (average SLOPE CV = 0.074%/month).

191

192   **2.5 Statistical analyses**

193   Data were processed in Microsoft Excel. Correlation analysis and Hierarchical Clustering of

194   Spearman correlation coefficients were performed in OriginPro 2023b. For the clustering,

195   Euclidean distances and group average clustering were used to draw the dendrogram. All

196   graphs in the manuscript were plotted in this software. Details on Multiple Linear Regression

197   (OriginPro 2023b) are detailed in the Supplementary Methods

198

199   **2.6 Ranking and Sensitivity Analysis**
200
201   Assay variables were ranked in Microsoft Excel, using the RANK.AVG function. Values were

202   ranked from the most desirable to least desirable value, depending on the favourable direction

203   of the assay, e.g., a high $T_{m,app}$ is desirable, whilst a low $T_{m,app}$ is undesirable.

204   For the sensitivity analysis, one formulation, e.g. A1, was removed from the dataset, the data

205   re-ranked as above and Hierarchical Clustering performed as stated in the main text. This

206   process was repeated sequentially for each formulation. The least significant correlations are

207   flagged in OriginPro, generally pertaining to branches within each assay group that have the

208   largest distance from the baseline, e.g., variables 30 and 32 in Figure S19. To further evaluate

209   the robustness of the assay variable groupings, the approach of Lu et al. was employed.[29] The

210   total number of times a variable paired with its immediate neighbour was counted in each

211   iteration of the analysis, then divided by the total number of iterations (10 in this case). Values

212   (termed P) close to 1 reflected the most robustly clustered variables (Figure S21).

213

2.7 Averaging of Developability Output Score (ADOS) algorithm

215   The foundations for the following analysis can be found elsewhere.[4,16] Firstly, the scores for a

216   formulation, i, in an assay variable, j, were scaled according to their position within the

217   distribution of the observed data (Equation 1)

$$V_{ij} = \frac{y - Y_{50\%}}{Y_{80\%} - Y_{20\%}}$$

219   Equation 1. where V_{ij} = scaled value, y = reported assay value, $Y_{50\%}$ = median, $Y_{80\%}$ = 80th

220   percentile value and $Y_{20\%}$ = 20th percentile value.

221   Next, the scaled values were normalised onto a best (0) to worst (1) scale (Equation 2a)

$$NV_{ij} = \frac{(V_{ij} - minV_{ij})}{(maxV_{ij} - minV_{ij})}$$

223   Equation 2a. where NV_{ij} = normalised scaled value, $minV_{ij}$ = smallest scaled value for the assay

224   variable and $maxV_{ij}$ = largest scaled value for the variable.

225   For assay variables where the smallest number corresponds to the worst score, e.g. the

226   formulation:mAb with the lowest Tm_{app} has the poorest thermal stability and a very negative

227   monomer-loss slope reveals faster aggregation or degradation, the scores were adjusted with

228   Equation 2b.

$$NV_{ij}^+ = 1 - NV_{ij}$$

230   Equation 2b. where NV_{ij}^+ = adjusted normalised scaled value.

231   Next, using the groups from Figure 4b, identified by Hierarchical Clustering, the average score

232   for a formulation across each group was calculated (Equation 3).

233
$$Grp\bar{x} = \frac{\left(\sum NV_{ij}^{(+)}\right)_x}{n}$$

234   Equation 3. where $Grp\bar{x}$ = averaged formulation score within assay group x, $\left(\sum NV_{ij}^{(+)}\right)_x$ = sum

235   of adjusted/normalized scaled values within assay group, x and n = number of assay variables

236   in group x. E.g. Group 1 (red group, Figure 4) has nine variables, thus n = 9 for this group.

237

238   Finally, using the approach of Jain et al.,[4] a 'distance from ideal' was calculated for each

239   formulation (Equation 4), which we term the Averaged Developability Output Score (ADOS).

240
$$ADOS = \frac{\left(\sum Grp\bar{x}\right)}{4}$$

241   Equation 4. where ADOS = the distance from ideal for each formulation and 4 = number of

242   assay groups.

243   By using this algorithm, then ranking the ADOS values on a best (lowest) to worst (highest)

244   scale, formulations which obtain low ADOS values across the assay groups are closer to 'ideal'

245   than those which obtain high values. Formulations with a high ADOS can thus be more

246   confidently deemed sub-optimal. The values obtained from Equation 3 can be weighted by

247   Multiple Linear Regression to obtain ADOS$_{MLR}$ (see Supporting Information, including Figure

248   S23).

249

250   **2.8 LASSO Regression on Ranked Data**

251

252   LASSO regression was initially performed to identify the minimal set of assays required to

253   predict the observed rate of change in % monomer at 25 °C. This was performed on the ranked

254   data using XLSTAT 2023. This method is independent to, and has a different mathematical

255   basis to the MLR approach and is ideally suited to datasets where there are more variables than

256   datapoints.[30] The 19 ranked assay variables (shown in Tables 3 and 4) were initially correlated

257   against the ranked rate of monomer-loss at 25 °C, using cross-validation to find the

258   regularisation parameter, λ, using the default settings (5 folds, 100 λ values) (Figure S24). This

259   analysis was subsequently repeated, using the 19 variables above or all the variables from

260   Tables 3 and 4 (including those in bold) to generate a predictive algorithm. An inherent strength

261   of LASSO is that it identifies only those variables that are important for the resulting model

262   (see Figure S24).

263

264   **Table 3: Summary of the variables output by the DAs (developability assays) employed**
265   **at t=0 on the formulation:mAb panel.** The colours of the variable ID number correspond to
266   Family Tree Group colour in Figure 4. Variables with ID numbers in bold were deemed
267   difficult to cluster and were removed from the final clustering dataset in Figure 4 (see Figure
268   S19).

Variable ID No.	**Assay**	**Variable**	**Abbreviation**
1	Rheology of 131 mg/mL sample	Viscosity	**Viscosity**
2	Hydrophobic Interaction Chromatography	Retention time (min)	**HIC**
3	Stand-up Monolayer Adsorption Chromatography	Retention time (min)	**SMAC**
4	Baculovirus Particle ELISA	ELISA signal (a.u.)	**BVP**
29 (removed from final dataset)	Affinity-Capture Self-Interaction Nanoparticle Spectroscopy	Plasmon wavelength shift (nm)	**AC-SINS**
5	Differential Scanning Calorimetry	1st apparent T_m transition (°C)	**DSC Tm1**

6		Apparent T_m of the Fab (°C)	**DSCTmFab**
7	Dynamic Light Scattering	Average hydrodynamic radius (nm)	**Rh (DLS)**
8		Diffusion interaction parameter k_D (mL/g)	**kD (DLS)**
30 (removed from final dataset)	Background Membrane Imaging	No of particles in t = 0 samples	**BMI Part**
9	High-performance size-exclusion chromatography (HP-SEC) at t=0	% monomer	**%mono HPLC**
10		Monomer retention time (min)	**Ret t mono**
11		% Higher Molecular Weight species	**%HMW (HPLC)**
31 (removed from final dataset)		% fragments	**%frag (HPLC)**
32 (removed from final dataset)	HP-SEC analysis of samples stressed in the Extensional Flow Device (EFD)	Observed rate of monomer loss at 0.25 mg/mL	**EFDv0.25mg**
27		Observed rate of monomer loss at 0.5 mg/mL	**EFDv0.5mg**
28		Observed rate of monomer loss at 1 mg/mL	**EFDv1mg**

269

270 **Table 4: Summary of the variables output by the *in silico* assays employed on the variable**
271 **domain sequences/homology models of mAb1, mAb2 and mAb3.** The colours of the
272 variable ID number correspond to Family Tree Group colour in Figure 4.

273

Variable No.	Assay	Variable	Abbreviation
12	CamSol algorithm	Structure-corrected CamSol Score	**CamSol**
13	Therapeutic Antibody Profiler (TAP)	Total CDR length (IMGT scheme)	**TAPCDRle**
14		TAP Patches of Surface Hydrophobicity	**TAPPSH**
15		TAP Patches of Positive Charge	**TAPPPC**
16		TAP Patches of Negative Charge	**TAPPNC**

Variable No.			
17		TAP Structural Fv Charge Symmetry Parameter	**TAPSFvCSP**

Table 5: Summary of the variables output from the accelerated and long-term stability study on the formulation:mAb panel. The colours of the variable ID number correspond to Family Tree Group colour in Figure 4.

Variable No.	Assay	Variable	Abbreviation
18	HP-SEC analysis of accelerated (AS) and long-term stability samples	Observed rate of change in % monomer at 5 °C	**MonoASv5C**
19		Observed rate change in % monomer at 25 °C	**MonoASv25C**
20		Observed rate of change in % monomer at 40 °C	**MonoASv40C**
21		Observed rate of change in % HMW species at 5 °C	**HMWASv5C**
22		Observed rate of change in % HMW species at 25 °C	**HMWASv25C**
23		Observed rate of change in % HMW species at 40 °C	**HMWASv40C**
24		Observed rate of fragmentation at 5 °C	**FragASv5C**
25		Observed rate of fragmentation at 25 °C	**FragASv25C**
26		Observed rate of fragmentation at 40 °C	**FragASv40C**

285 **Results**

286 **Assessing the developability and kinetic storage stability of a panel of antibody**
287 **formulations.**

288 The formulation:mAb panel comprised three IgG1s: mAb1, mAb2 and mAb3 in three different

289 buffers selected to reflect typical marketed product formulation compositions[31] (20 mM L-His

290 + 190 mM L-Arg pH 6.0 (Buffer A), 20 mM L-His + 7.5% (w/v) sucrose, pH 6.0 (Buffer B)

291 and 25 mM sodium citrate pH 5.0 (Buffer C)). The mAbs were dialysed into these buffers,

292 diluted to a final concentration of 50 mg/mL, spiked with 0.02% (w/v) Polysorbate 80 (PS80)

293 and vialled (Methods), yielding nine formulation:mAb samples, A1–C3 (with the letter

294 identifying the buffer and the number the mAb identity, e.g. B2 is mAb2 in Buffer B (His-

295 sucrose), Table 1, Methods).

296

297 Each of the nine formulation:mAbs were initially characterised using ten different DAs (Figure

298 1, Table 3, Methods and Supporting Information,). These were selected to characterise a broad

299 array of different biophysical features as evidenced by their inclusion in different branches of

300 hierarchical clusters of DAs reported by Jain et al[4] or, for assays not included in the Jain study,

301 their published ability to provide additional insight or prediction of mAb developability (e.g.

302 Diffusion interaction parameter (*kD*) and the Extensional Flow Device (EFD), see below). The

303 assays, grouped by the biophysical property being probed and the number of output variables

304 measured by each technique, are briefly described below and more fully (together with a

305 identification number used herein) in Table 3. Group (I) probes Colloidal stability: viscosity of

306 the concentrated, surfactant-free formulations (yielding 1 variable (var.) output), retention

307 times in size exclusion- (SEC), hydrophobic interaction- (HIC), and stand-up monolayer

308   adsorption chromatography (SMAC) (each yielding 1 var.), affinity-capture, self-interaction

309   nanoparticle spectroscopy plasmon wavelength shift (AC-SINS) (1 var.) and dynamic light

310   scattering (yielding 2 var., the hydrodynamic radius and the kD). Group (II) probes thermal

311   stability by differential scanning calorimetry (DSC) (2 var. the first and apparent Fab melting

312   temperature) while Group (III) probes miscellaneous features of the molecules: Baculovirus

313   particle adsorption, linked to rapid *in-vivo* clearance[32] (BVP) (1 var.), the number of sub-visible

314   particles present by background membrane imaging (BMI) (1 var.) and, finally, the rates of

315   monomer loss induced by the Extensional Flow Device (EFD) at 0.25-, 0.5- and 1 mg/mL (3

316   var.). This device, developed at Leeds,[16,26–28] subjects proteins to the potentially synergistic

317   stresses of hydrodynamic flow fields and interfaces that are experienced by proteins throughout

318   their manufacture, including depth filtration and fill-finish steps.[33] The EFD provides unique

319   insight relative to other assays, [16,26,27] suggesting its utility as a complementary DA to those

320   commonly employed by the biopharmaceutical industry.[16] The use of this assay is explained in

321   detail in the Methods. These experimentally derived variables were augmented with further

322   variables (Group (IV)), derived from *in silico* methods (Table 4): prediction of CDR and F_V

323   liabilities using Therapeutic Antibody Profiler[8] (5 var.) and the structure-corrected solubility

324   of the variable domains using CamSol[5] (1 var.).

325   Exemplar data, together with violin and box plots for all nine formulation:mAbs, are shown for

326   each DA in Figures S1–12 together with a description of each assay (Supplementary Methods).

327   Generally, most DAs produced non-normally distributed populations with long tails, as

328   observed previously[4,16] and the relationship between DA outputs is often difficult to rationalise.

329   For example, the viscosity of formulation:mAb B2 was four times above the upper limit

330   typically acceptable for prefilled syringe administration[34] (Figure S1) and showed evidence of

331   aggregation by DLS (Figure 2a). Despite this, *in silico* analyses failed to flag liabilities in the

332   variable domains of this and the other mAbs which could lead to colloidal instability (Figures

333   S7 and S8).

334

335

336
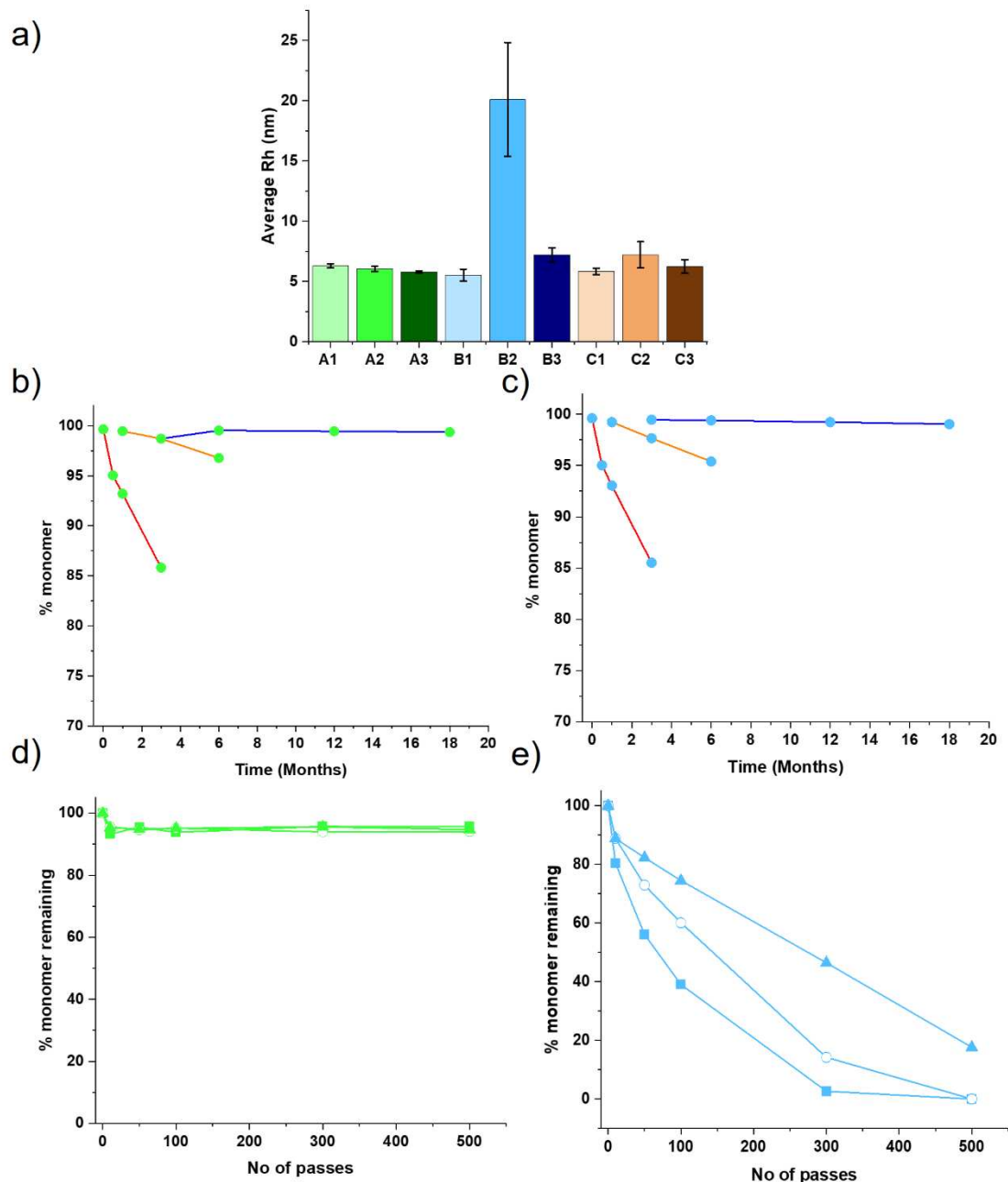
Figure 2. Using the 'developability toolkit' to screen antibody formulations. a) Average hydrodynamic radius (R_h) of the nine samples in the study, obtained using dynamic light scattering, measured at concentrations between 2–20 mg/mL (Supplementary Methods and Figure S5). Bars are coloured according to the formulation:mAb, error bars = s.d. b) and c) HP-SEC analysis of formulation:mAbs A2 (mAb2 in histidine-arginine) (b) and B2 (mAb2 histidine-sucrose) (c) following accelerated and long-term storage stability (Methods). Samples were incubated at 50 mg/mL for the times and temperatures indicated, with the relative % monomer in HP-SEC trace quantified. Lines through the points at 5 °C (blue), 25 °C (orange) and 40 °C (red) are guides to the eye, not fits to the data. d and e) HP-SEC analysis for formulation:mAbs A2 (d) and B2 (e) following stress in the EFD (Methods). Initial [protein] in EFD experiments = 0.25 mg/mL (squares), 0.5 mg/mL (open circles) and 1 mg/mL (triangles), with % monomer remaining quantified by HP-SEC (Methods).

18

350   To obtain kinetic stability data for each of the characterised formulation:mAbs, we incubated

351   the vials under accelerated stability (AS) conditions at 40 °C, as well as long-term storage

352   (LTS) conditions at 25 °C and 5 °C. Vials were removed from the incubators after: two weeks

353   (0.5 months), 1 month and 3 months at 40 °C; 1-, 3- and 6 months at 25 °C and; 3-, 6-, 12- and

354   18 months at 5 °C (Methods). While HP-SEC was used to quantify the relative amount of

355   monomeric, higher order (high molecular weight, HMW) and fragmented mAbs injected onto

356   the column, the total soluble protein concentration was additionally quantified using UV-

357   visible spectroscopy with 350 nm correction to remove scattering artefacts (Supplementary

358   Methods, Figure S13). Together, these analyses showed that the majority of samples formed

359   soluble HMW species and fragments over the course of the AS and LTS studies but

360   formulation:mAbs C2 and C3 formed insoluble aggregates after incubation for three months at

361   40 °C (Figure S13 biii and ciii, respectively), resulting in the removal of these points from the

362   observed rate of monomer-loss analysis.

363   The observed rates of change in % monomer, HMW species formation and fragmentation

364   (quantified by HP-SEC,[35] Methods), for each formulation at each temperature, were calculated

365   using linear regression (Methods). These data, shown in the Supporting Information (Figures

366   S14–17) comprise Group (V) in our suite of DAs (Table 5). A decrease in the amount of

367   monomer was accompanied by the concomitant increase in the HMW species and fragments

368   detected within each sample (Figures S14–17). Generally, incubation at higher temperatures

369   accelerated monomer loss for all the mAb samples (Figures 2b and c, for example), with these

370   rates becoming thirty and two hundred times slower at 25 °C and 5 °C, respectively (based on

371   the median rate for all nine formulation:mAbs, Figures S18). In accord with other studies,[36–

372   38] this process cannot be described by simple Arrhenius kinetics,[36,37] obviating the use of

373   recently developed kinetic models[39–41] to predict the LTS/ shelf-life for these

374   formulation:mAbs. Under the conditions and buffers used here, all formulation:mAbs showed

375   minimal degradation at 5 °C (~0.01–0.09% monomer /month, Figure 3) precluding the use of

376   these data as our metric of manufacturability, given the relative size of the experimental and

377   fitting error compared to the datapoints (average coefficient of variation = 0.074% /month,

378   median rate of loss = 0.015% /month, Methods Section 2.4). By contrast, degradation rates

379   were approximately ten times faster at 25 °C (Figure 3), and consequently these data were used

380   to rank formulations as the error (0.036% /month) was far smaller than measured rate of loss

381   (median rate of loss = 0.34% /month). We note here that at 25°C formulation:mAbs C2, B2

382   and C1 exhibit statistically significant different rates to each other and also to A3 and B3 (which

383   exhibit indistinguishable rates) and A1, B1, A2 and C3 (which display varying difference in

384   significance to each other but are distinct to A3 and B3 and C2, B2 and C1). For simplicity,

385   we first describe our analyses using a ranking based on the observed rate values (i.e. left to

386   right in Figure 3d ranks formulation:mAbs from best to worst). We then show how changing

387   the ranks for A1, B1, A2 and C3 has minimal effect on the resulting outputs, validating the use

388   of this dataset as our test example for the statistical workflow presented herein.
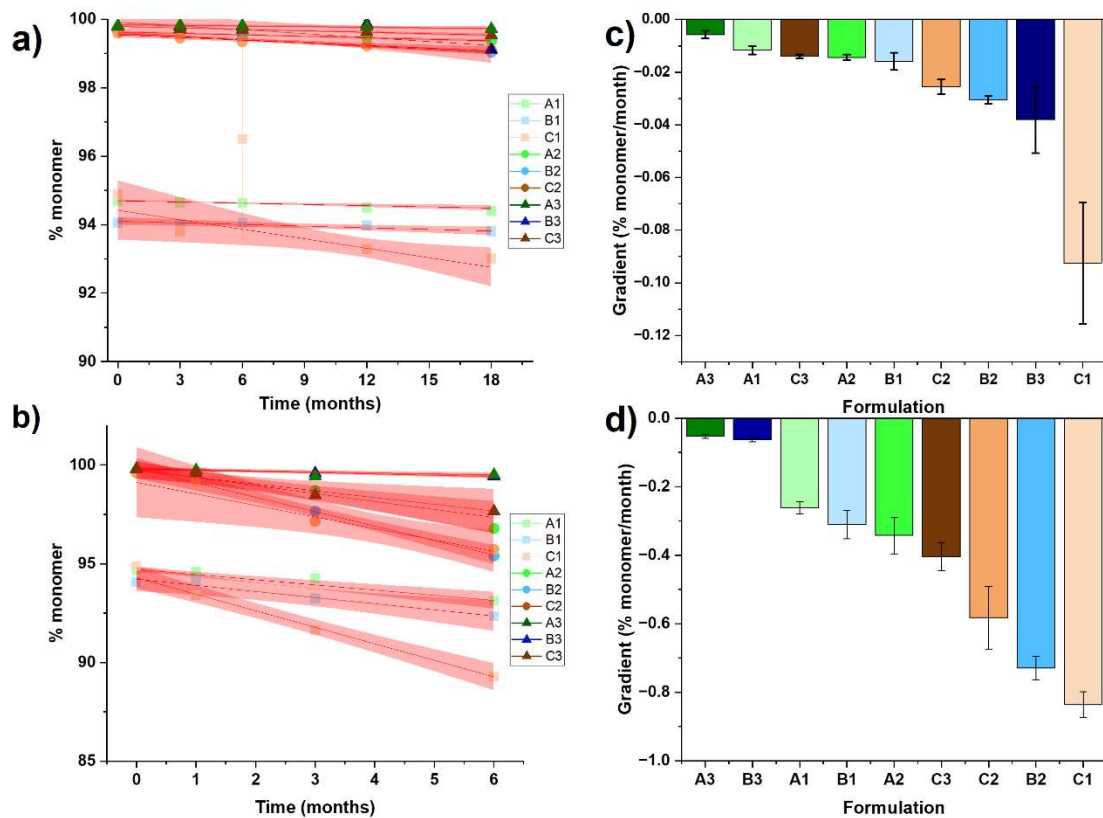
Figure 3. Change in % monomer over 6 to 18 months at 25 °C and 5 °C, respectively. *%
monomer calculated for formulation:mAbs A1–C3, derived from technical repeats at 5 °C (a)
and 25 °C (b). Fitting a straight line to the data yields the observed rate (gradient) alongside a
standard error. Red region = 95% confidence interval. Observed rates for the nine
formulation:mAbs at 5 °C (c) and 25 °C (d); error bars = standard error.*

Statistical analysis reveals the relationships between the developability assay variables.

The first aim of this study was to determine the relationship between the outputs of each

variable, obtained from the suite of DAs used, to allow the selection of a reduced set of

complementary, non-degenerate DAs. To do this, we performed Spearman's rank analysis of

the variables, followed by Hierarchical Clustering of the resulting correlation coefficients, as

described in previous studies.[4,12,16,19] As more than one variable can be obtained from some of

402   DAs used here (e.g. the hydrodynamic radius (R_h) and diffusion interaction parameter (kD) are

403   both obtained from DLS), a total of 32 assay variables for each of the nine formulation:mAbs

404   (referred to as samples herein) were analysed (see Tables 3–5, Figure 1), generating a

405   Spearman's rank correlation coefficient for each pairwise variable combination. These values

406   were then subjected to Hierarchical Clustering analysis, as described previously[4,16] (Figure

407   S19a), yielding six branches each containing variables that are related by the information they

408   provide (Figure S19b). To better understand the strength of the clustering, the least significant

409   (longest distance from baseline) assay variable in each branch was noted (Supplementary

410   Methods). Following this, the data obtained for each formulation:mAb (A1–C3) was iteratively

411   removed from the panel and the analyses described above repeated. Repeating this process for

412   the remaining nine combinations of samples (i.e. the dataset comprising all formulations plus

413   nine datasets with one formulation:mAb removed from each) allowed the identification of

414   variables which clustered poorly with other assays. Using this approach, four variables,

415   approximately equivalent to removing one formulation:mAb, were found to be the least

416   significant branch assay in at least six dendrograms in the analysis, suggesting that these

417   variables were distinct in the information they provided. As the first aim of this study was to

418   understand degeneracy within DAs, these variables (AC-SINS (var. 29), BMI (var. 30), initial

419   levels of fragmentation by HP-SEC (var. 31) and the observed rate of EFD-induced monomer

420   loss at 0.25 mg/mL (var. 32)) were removed from the analysis.

421   Hierarchical Clustering of the pairwise Spearman's correlation coefficients was repeated on

422   the remaining 28 variables obtained from 10 DAs (Tables 1-3) for the nine formulation:mAbs

423   and identified four branches of related assay variables (Figure 4a and b). The red cluster is the

424   largest, comprising nine variables (variables 1, 5–8, 16 and 20–22), probing several molecular

425   features including the viscosity (variable 1), thermal stability (variables 5 and 6) and observed

426   rate of monomer loss at 40 °C (variable 20). The relatedness of these latter two assays makes

427   mechanistic sense: poor thermal stability may result in the promotion of unfolding and

428   aggregation *via* the unfolded state at elevated temperature.[42,43] The blue cluster (8 variables)

429   comprises many of the TAP metrics (variables 13–15 and 17), as well as measures of molecular

430   'stickiness'[44] (HIC, SMAC and BVP, variables 2–4). The smallest green cluster of five

431   variables (9, 11,12, 24 and 26) probes miscellaneous features, including the observed rate of

432   fragmentation at 40 ˚C (variable 26). The final purple cluster contains six variables (variables

433   10, 18, 19, 25, 27 and 28). Notably, this includes the observed rates of monomer loss at 5 °C

434   and 25 °C (variables 18 and 19, respectively) which stem from the same branch, as do the

435   observed rates of monomer loss in the EFD at 0.5- and 1 mg/mL (variables 27 and 28,

436   respectively). The robustness of these relationships was further assessed by sequentially

437   removing the data obtained from each formulation:mAb from the dataset, which was then re-

438   ranked and re-analysed (example dendrograms in Figure S20).

23
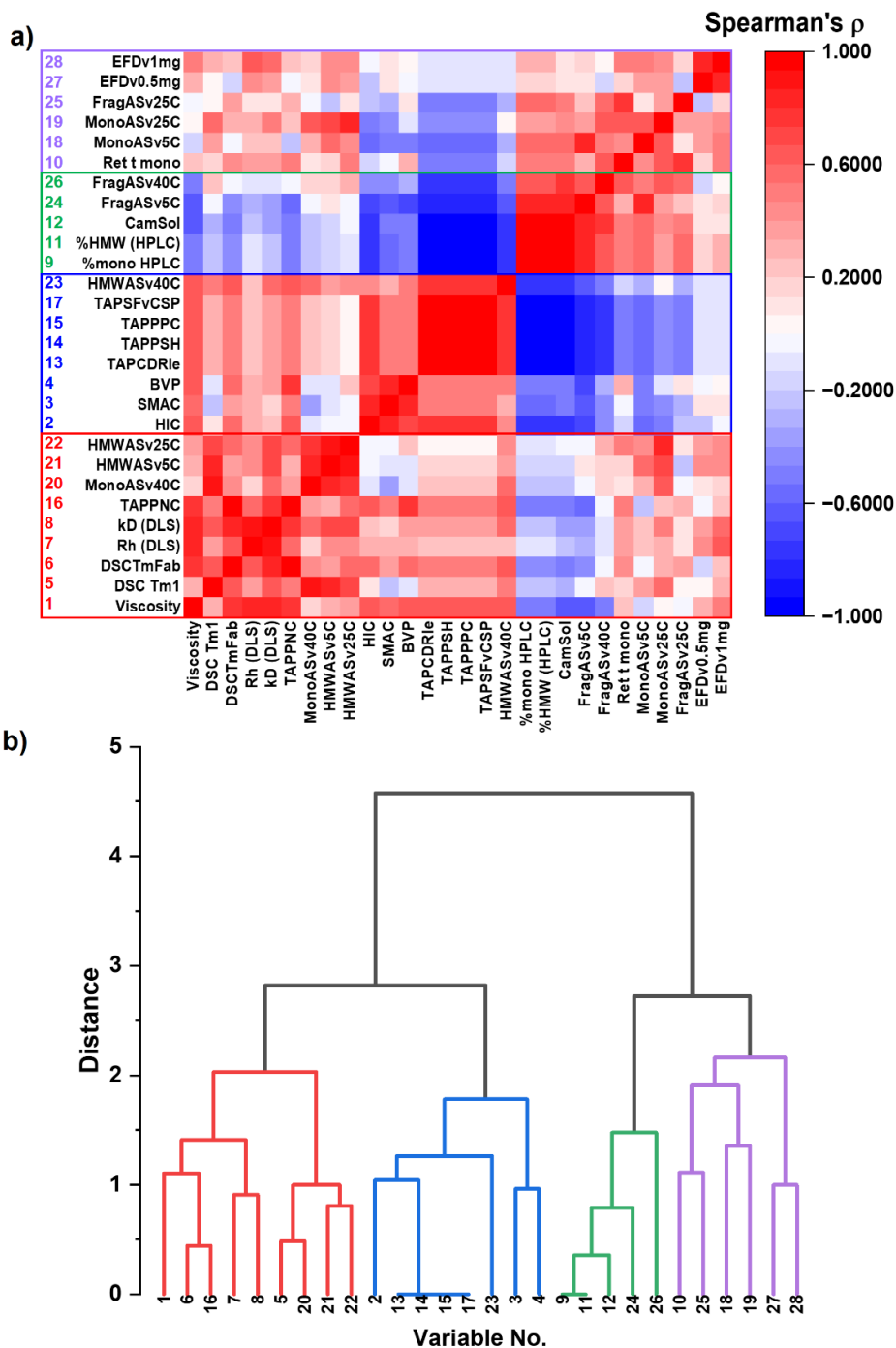
Figure 4. Statistical analysis clusters assay variables in the developability "assay pool". a) Heatmap of Spearman's rank correlation coefficients (ρ) for the pairwise interactions between the 28 best-clustered assay variables in the dataset. b) Hierarchical Clustering analysis of these variables generates a "Family Tree" comprising four branches of related assays. The observed rates of monomer loss after stress in the EFD at 0.5- and 1 mg/mL (variables 27 and 28, respectively) are in the same branch (purple) as the equivalent rates following storage stability at 5°C and 25 °C (observables 18 and 19, respectively). The assays from which the variables are derived, and their abbreviations are listed in Tables 3–5.

24

449   To quantify the differences in the dendrograms, we used the approach of Lu et al[29] and

450   calculated the frequency with which an assay variable paired with its immediate neighbours

451   over all iterations, with a median "P-value" of 0.9 (P-values range from 1 (no change in pairing)

452   to 0 (all pairings changed), Figure S21). For reference, 10 of 28 variables did not change

453   pairing at all, with 11 of 28 changing 1 or 2 times (Supplementary Methods and Figure S21).

454   At a coarser level, an assay was found to be assigned to a different group (branch) only 5 of 28

455   times (median P = 1). Small changes in assay groupings for subsets of antibody samples have

456   been observed previously.[4,16]

457

458   **Developability assay outputs can be condensed into a single metric.**

459   Each cluster of DAs provides assessment of distinct biophysical properties (and critical quality

460   attributes) which together determine developability. We thus asked how one could rationally

461   combine DAs to obtain a consensus measure of developability to integrate the often-conflicting

462   results of the DAs employed (Figure 5).

463
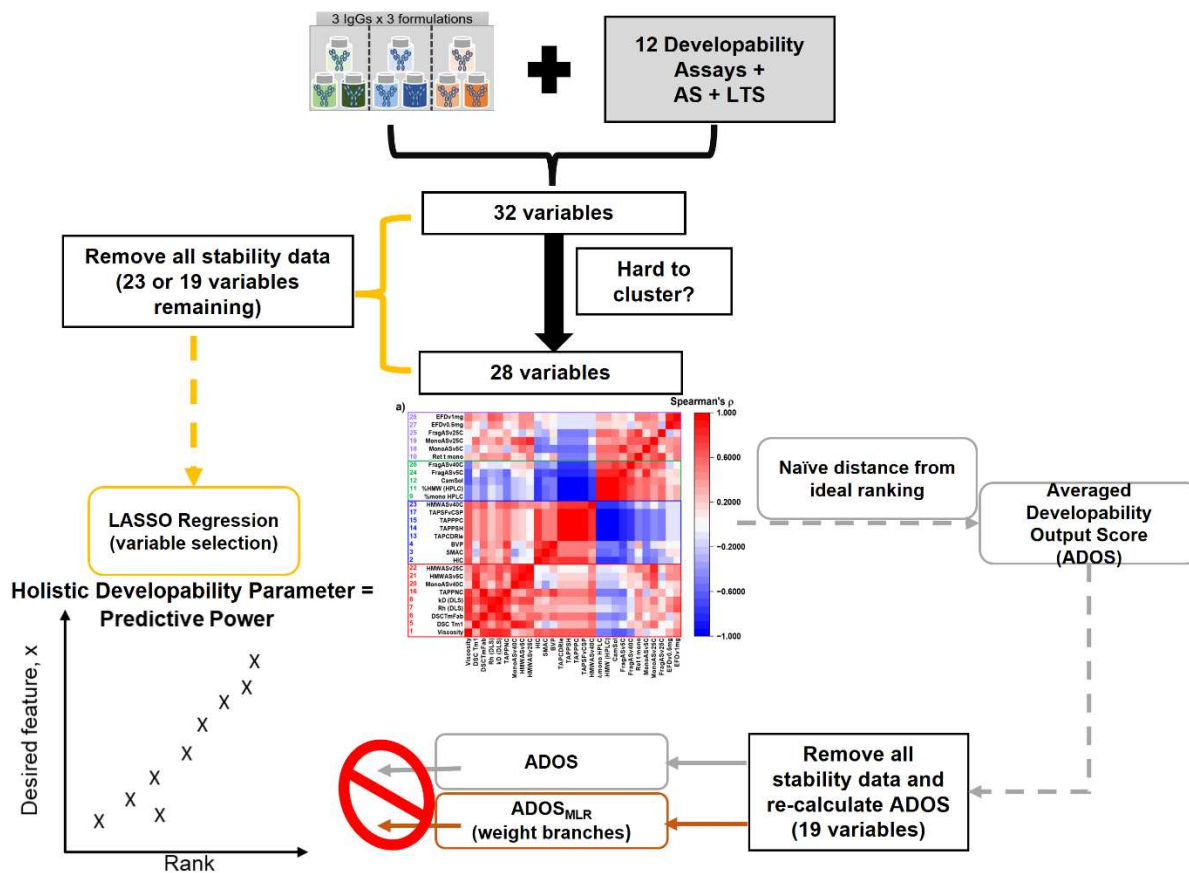
Figure 5. Statistical analysis of the dataset yields a Holistic Developability Parameter (HDP). Spearman's rank and Hierarchical Clustering identifies the best-clustered set of 28 variables. One can naïvely compute an Averaged Developability Output Score (ADOS) from these assay groups to holistically rank formulations (silver arrows). This method is a poor protector of a desired feature (storage stability at 25 °C here). Multiple Linear Regression (MLR) can be used to optimise ADOS but uses the outputs of all assays (thus we have more variables than data points). An alternative approach uses Least Absolute Selection and Shrinkage Operator (LASSO) regression to identify which variables contribute to the prediction of the desired feature, as stated above. These key variables make up the HDP.

473

Inspired by the work of Jain et al.,[4] where a 'distance from ideal' of each test formulation:mAb for each DA was derived, we adapted this analytical framework to generate a parameter to summarise the overall performance of a candidate during developability assessment. For a given variable, each formulation:mAb was ranked on a best (0) to least favourable (1) scale (Methods). The average score for the assay variables in each branch is then calculated, and the

26

479   sum of the average values of each branch calculated. In this model-independent approach,

480   formulation:mAbs with a lower score (herein termed Averaged Developability Output Score,

481   ADOS) are expected to have more quality attributes for developability. This approach firstly

482   identifies mAb2 as likely to be difficult to develop, as it scores badly in most assay clusters,

483   irrespective of buffer condition (Figure 6ai) and secondly, identifies Buffer A (histidine-

484   arginine) as the best formulation. One could thus utilise ADOS to consolidate the data from a

485   variety of assays into one, easy-to-interpret metric, reducing the likelihood of one assay

486   variable leading to the outright rejection of a given formulation.

487

488
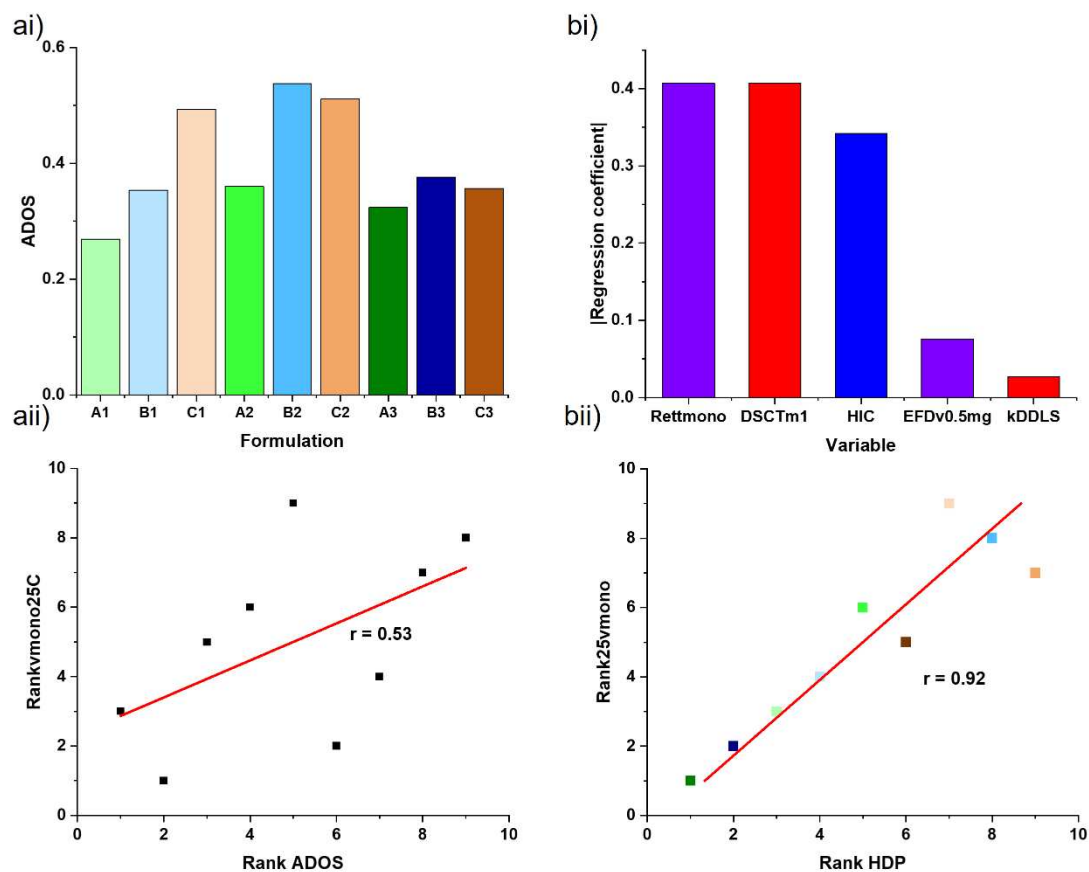
Figure 6. ADOS identifies favourable mAb formulations, while the HDP identifies the "most developable". ai) ADOS, derived using the 28 best clustered variables from Figure 4. Bars are coloured by formulation. The ADOS outputs can be put on a rank scale to aid other analyses (Supporting information) aii) Rank of observed rate of change in % monomer at 25 °C vs ranked ADOS score. A linear fit to the data shows a modest correlation (r = 0.53). LASSO regression of the variable dataset excluding accelerated and storage stability (Group V) data identifies the five assay variables (bi) that together yield the Holistic Developability Parameter which correlates strongly with the ranked observed rate of change in % monomer at 25 °C (r = 0.92) (bii). These five diverse assays (abbreviations defined in Tables 3–5) are colour-coded in accord with the dendrogram in Figure 4b.

ADOS cannot be used to assess storage stability

While this method yields values that correlate qualitatively with empirical knowledge of the buffers and mAbs used, its ability to identify formulation:mAbs with favourable short-/long-term storage stability was unknown. The prediction of kinetic stability at 5 °C is highly desirable, as this is both expensive in terms of material and time. However, the slow degradation kinetics for the samples studied here precludes this goal for this dataset (see Discussion). To answer this question, we thus chose the rank order of change in % monomer at 25 °C as the "measured attribute of manufacturability" to be predicted; but we note that other user-defined critical quality attributes could also be used. As all the accelerated and storage stability data in Group V (obtained at 5 °C, 25 °C and 40 °C) are expensive in terms of protein required and time to obtain, all Group (V) data were removed from the dataset, allowing only rapid "t=0" DAs with low sample requirements to be used to predict storage stability. The remaining 19 variables in the dataset were re-analysed by Spearman's rank and Hierarchical Clustering, yielding the same four assay clusters identified previously (Figure S22). Plotting the ranked, observed rate of change in % monomer at 25 °C versus the ADOS calculated using the clusters derived from these 19 variables, results in a weak correlation (Pearson's r = 0.53, Figure 6aii). As each branch (and assays within branches) may not have equal importance in determining storage stability, Multiple Linear Regression (MLR, Supplementary Methods) was employed to weight each branch according to its contribution to this prediction. This made the correlation markedly better (Pearson's r = 0.93, Figure S23), with the caveats that the

29

525   ADOS$_{MLR}$ is still derived from many different assays, resulting in more degrees of freedom

526   (i.e., variables) than data points.

527

528   **LASSO regression can be used to identify key predictor variables**

529   Whilst the described approaches provide an understanding of the inter-relationship between

530   assays and assay clusters, reducing the number of DAs still requires *ad-hoc* decisions to be

531   made on the dataset or a large panel of DAs to be included within the regression against the

532   chosen developability parameter. To obviate this requirement, we adopt a systematic approach

533   which identifies the smallest set of variables to link DAs with the chosen measurable attribute

534   of manufacturability. Least Absolute Shrinkage and Selection Operator (LASSO) regression

535   is a variable selection method which reduces the number of variables to the minimum set which

536   best fit the data, with this method being useful when there are more variables than samples (our

537   dataset comprises 19 variables and nine samples, Supplementary Methods).[30] Performing

538   LASSO regression on the dataset without Group (V) data reveals that just five assay variables

539   can predict the ranked absolute observed rate of change in % monomer at 25 °C (r = 0.92,

540   Figure S24, Figure 6b). These variables are the first apparent thermal transition in DSC and the

541   *kD* obtained from DLS (Red group, variables 5 and 8, respectively), monomer retention times

542   on HP-SEC (Purple group, variable 10) and HIC columns (Blue group, variable 2) and the

543   observed rate of monomer loss induced by the EFD at 0.5 mg/mL (Purple group, variable 27).

544   Though the regression coefficient for the *kD* is small, removing it from the dataset results in

545   no correlation being obtained from LASSO, reinforcing the importance of the *kD* as a

546   developability parameter.[23] As no information derived from Hierarchical Clustering is used in

547   LASSO regression we repeated this procedure on the full DA dataset (not including the AS or

548   LTS (Group V) data) as the four difficult to cluster variables (29–32) may still provide

549   important information through their unique insight. LASSO regression once again showed high

550   correlation with change in % monomer at 25 °C (Pearson's r = 0.95, Figure S24c) but required

551   six variables: the same five as above and one of the difficult to cluster variables omitted in

552   previous analyses: the number of particles observed in the formulation:mAbs at t=0 by BMI,

553   variable 30).   Intriguingly, repeating this process to predict the rank order of accelerated

554   stability (% monomer at 40 °C), yielded a lower Pearson's r (0.86) with LASSO regression

555   only selecting the 1st transition by DSC as an important variable for this (Figure S24c). This

556   together with non-Arrhenius degradation kinetics, suggests that monomer loss may occur by

557   different mechanisms at 25 °C and 40 °C. As noted above, error analysis of the linear regression

558   of the 25 °C degradation rate (Supplementary Methods and Figure 3) showed that A3 and B3

559   have very similar rates of monomer loss at 25 °C and A1, with B1, A2 and C3 displaying

560   varying degrees of significant difference between the observed rates (Figure 3d). To investigate

561   the effect of fitting error on formulation:mAb ranking, the ranks of A3 and B3 were assigned

562   tied 1st (i.e., most stable), with C2, B2 and C1 (all significantly different to every other

563   formulation:mAb) assigned fixed ranks of 6th, 7th and 8th, respectively.   The remaining four

564   formulation:mAbs were systematically re-assigned ranks 2–5 using every combination of each

565   of their maximal (high, H) and minimal (low, L) degradation rates, calculated from the fit

566   error, yielding 16 different (2^4) ranks from LLLL to HHHH. Generally, irrespective of whether

567   the full or focussed variable dataset was used for LASSO regression, the predictive power

568   (Figures S25 and S26) and identified keystone variables (Figure 7) are preserved.   As a median

569   of six keystone variables, which probe diverse physicochemical features of the molecules, are

570   selected from these analyses, (Figure 7), this suggests our approach, which generates a Holistic

571   Developability Parameter (HDP) could work as general strategy for mAb developability.

a)

Best-clustered variables

b)

By cluster group
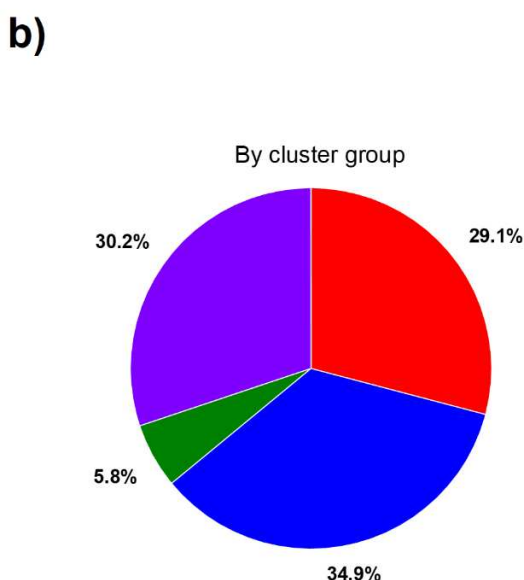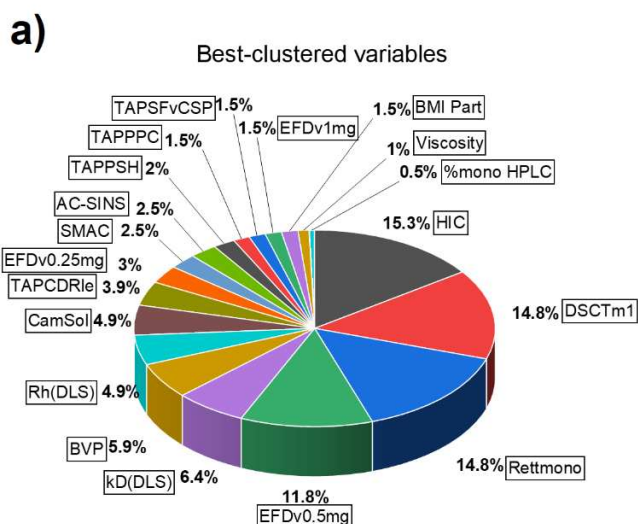
Figure 7. Robustness analysis of the 25 °C storage stability dataset and its impact on the LASSO regression. a) Pie chart showing the selection frequency of the 19 best-clustered variables, which were selected by LASSO regression over the 17 (absolute plus 16 combinations of ranks for A1, B1, A2 and C3) 25 °C data ranks. The five most frequently selected variables are the same as those in Figure 6bi. b) Pie chart showing the selection frequency of variables in a) grouped and coloured according to the dendrogram in Figure 4. Each LASSO iteration mainly selects variables from the red, blue and purple assay groups. 5 to 6 core "t=0"developability assays, spanning an array of physicochemical features, are sufficient to predict 25 °C storage stability.

Discussion

An ever-expanding toolkit of developability assays has been established by the field to interrogate various physicochemical features of antibodies, with a view to identifying lead candidates with favourable drug-like properties.[2,4,45] Studies have subjected panels of IgG antibodies[4,7,12,20,46–48] and other modalities [19,49] to various established[9,50,51] and novel DAs[13,17] and analysed the resulting datasets by a variety of statistical methods including Pearson's[12,19] and Spearman's correlation.[4,16,49] The majority of these studies have investigated the relationship (and potential redundancies) between different DAs including a wide array of well used assays[4] or the relationship between these established DAs and novel assays that report on hydrodynamic and interfacial stability[12,13,16] or in silico-derived parameters.[47] Other groups have examined the ability of DAs to predict the behaviour of proteins during downstream processing.[20,23] Interestingly, and in agreement with our results, both of these latter studies identified parameters that measure self-association such as k_D, to be the strongest predictors. Despite these successes, a framework for the integration of the diverse outputs of DAs was lacking. This challenge is non-trivial, based on the array of mAb sequences available,[45] the orthogonal set of assays one can use to interrogate these molecules[2,47] and the impact that different formulation components (namely buffers, co-solutes and excipients) can have on the above.[31]

We subjected a panel of three mAbs in three different formulations, to an array of DAs and measured their accelerated and long-term stability over a three to 18-month period. Spearman's

603   rank was chosen to assess correlations between the resulting assay variables, as this avoids the

604   potential bias from assuming linear correlations between different variables and reduces the

605   influence of measurement noise on the analysis.[52] By employing Hierarchical Clustering on

606   the Spearman correlation coefficients, we were able to identify DAs which group readily into

607   families (e.g. HIC and BVP), as well as four DAs which were hard to cluster (AC-SINS, BMI,

608   initial levels of fragmentation by HP-SEC and the observed rate of EFD-induced monomer loss

609   at 0.25 mg/mL). For AC-SINS, poor clustering may be due to the atypical blue-shifts observed

610   in Buffer B (Figure S4, possibly caused by a change in the stability of the nanoparticles

611   themselves).[53] For the EFD data, we postulate that surface-dominated aggregation occurs at

612   low protein concentrations with a second bulk aggregation pathway occurring at higher

613   concentrations (Figure S11).[28] It is important to note that "difficult to cluster" may instead

614   indicate that these assays probe unique features of the molecules as shown when the outputs of

615   the EFD assay applied to subset of the "Jain" panel of mAbs were compared to the other DAs,[16]

616   as well as outputs derived from charge-stabilised self-interaction nanoparticle spectroscopy and

617   poly-specificity particle assays performed on a set of 80 clinical-stage sequences.[46]

618   We utilised 12 DAs at t=0, as well as performing a stability study at three temperatures (5-, 25-

619   and 40 °C) for 18-, 6- and 3 months respectively. While we did monitor the change in the

620   macroscopic properties of the samples using visual inspection standards,[54] the non-continuous

621   nature of the data generated precluded their inclusion in our final workflow. Furthermore, the

622   particulate matter was tracked over the course of the stability study using background

623   membrane imaging. Many 40 °C samples exceeded the recently derived [55] measurement limits

624   for the technique after just 1 month (data not shown), hence only the t=0 data were used in the

625   final dataset. Transforming the outputs of the 28 best-clustered variables from these assays to

626   a single scale allowed us to understand how best to utilise these data. Firstly, by assuming all

627   assays are equally important, we condensed the complex and sometimes conflicting DA outputs

628   to a single measure of biophysical behaviour (the ADOS), in a similar fashion to the 'distance

629   from ideal' measurement derived by Jain et al. 2017, though other normalisation methods have

630   been developed recently.[51] The distance from ideal values were used by Jain et al. to then

631   cluster the 137 IgG molecules in their study into groups of well-behaved (i.e., developable)

632   sequences, as well as those with less favourable properties, without explicitly ranking these

633   from best to worst or investigating the consequences of 'non-developability' on kinetic

634   stability, for example. Rattray and colleagues condensed their DAs using a normalisation

635   method, summing these scores but attributing no weighting to e.g. different families of assays,

636   as hierarchical clustering was not employed on their ranked data. They showed that a lower

637   normalised score correlated with reduced viscosity for a panel of high concentration mAbs.[51]

638   The ADOS method identified the arginine-containing Buffer A as the formulation that yields

639   the best-behaved molecules (in terms of biophysical properties), but it is a poor predictor of the

640   exemplar used to test our manufacturability prediction, that of kinetic stability at 25 °C. This

641   is probably because inherent within the ADOS methodology is the assumption that all assays

642   within a branch and all branches are equally important. Using a similar approach Wolfgang

643   Freiss and colleagues showed that a modest correlation was observed between aggregation after

644   six months at 4 °C and 25 °C (the data for both temperatures and all formulations was averaged)

645   and a "Stability Risk Score By High Analytical Effort" derived from 16 variables.[19] Similarly

646   to the ADOS approach, this work also suggested that the formulation largely determined the

647   output score.[19] By essentially removing unimportant variables (in terms of predictive power),

648   LASSO regression, is a powerful method to identify the subset of assay variables and optimise

649   the weightings necessary to predict kinetic stability at 25 °C. In contrast to the multiple studies

650   to delineate the relationship between DAs, studies investigating the relationship between DAs

651   and kinetic stability at 5-, 25- and 40 °C are less common. Goldberg et al., assessed DAs such

652   as Tm,app and aggregation onset temperature and 40 °C aggregation and monomer-loss rates

653   for a panel of mAbs in different formulations. They found the strength of the correlation was

654   dependent on the formulation condition and that the correlation with 40 °C and 4 °C data was

655   poor.[38] Others have also shown it is difficult to correlate behaviour of different DAs with real-

656   time stability, based on the molecules and formulations in questions and the temperature-

657   dependence of their underlying degradation mechanism.[19,21,49]

658   Comparing the outputs from the independent approaches of hierarchical clustering and LASSO

659   regression shows that HDP integrates variables from different branches of the "family tree" of

660   clustered assays, which report on a range of biophysical properties: thermal and colloidal

661   stability (Tm1 by DSC and k_D by DLS), stickiness (HIC and SEC retention time) and sensitivity

662   to interfacial and hydrodynamic stresses (EFD). The emergence of colloidal stability accords

663 with a wealth of previous studies that links this property to downstream processing and solution

664 behaviour.[20,23,51]. The non-Arrhenius kinetics exhibited by our formulation:mAbs and reported

665 in other studies,[36–38] prevents the use of recently established kinetic models to directly predict

666 long term stability from our accelerated stability data.[39–41,56,57] and also suggests that

667 aggregation (or any other process that drives the monomer loss used as metric of

668 manufacturability used here) may be driven by transient partial unfolding of the native state.

669 This accords with monomer loss increasing with decreased Tm1, increased HIC and SEC

670 retention time and increased sensitivity to interfacial and hydrodynamic stresses. Given this

671 broad sampling of biophysical characteristics and its strong correlation with the ranked stability

672 data obtained at 25 °C we have termed this the Holistic Developability Parameter or HDP. The

673 fact that our developability framework, which utilises many diverse assays, was able to

674 describe this correlation suggests that monomer loss occurs by distinct pathways that do not

675 simply involve global unfolding and that the generality of our approach removes the need for

676 the user to have a detailed knowledge of the aggregation mechanism underpinning a given

677 protein's degradation pathway.[42] Similarly, as the HDP is determined by diverse assays (i.e.

678 four of the five families of related assays, Figure 6), these assays may be sufficient to broadly

679 define the biophysical and chemical behaviour of proteins. Consequently, the same core assays

680 may be sufficient to predict a variety of critical quality attributes but using a HDP comprising

681 different weightings for each assay. The prediction of 5 °C long-term storage stability using

682 LASSO was precluded by the stability of the formulation:mAbs in our test set at   this

683   temperature. This may be because the mAbs used in our study (and others[21]) had all reached

684   later stages of development. Accordingly, we suggest that the method we describe is employed

685   as a rapid screen during candidate selection to ensure identification of mAbs with suitable long-

686   term stability after sequence-based features which are linked to inherently poor developability,

687   e.g. charge and hydrophobicity[58], or low chemical stability are removed using online tools such

688   as LAP.[59] Here, we have focussed on predicting kinetic stability at 25 °C, as this parameter is

689   onerous to measure in terms of time (six months) and material (>200 mg per molecule). We

690   reiterate that our approach provides a general framework to define the key assays which predict

691   any measure of manufacturability of the user's interest, provided a test dataset of the outputs

692   of a variety of DAs, together with the parameter of interest to be predicted, has been measured

693   for a panel of mAbs. Here, in contrast to more complex machine-learning methods (which may

694   nonetheless employ LASSO regression), we have used a relatively small dataset and LASSO

695   regression to generate a simple and sparse predictive model containing five or six key variables,

696   using assays which consume milligram quantities of material and take less than a day to

697   complete. Furthermore, these variables stem from different branches of the "family tree" of

698   assays, thus encompassing a range of biophysical features of each formulation:mAb. Of course,

699   more molecules, covering number, sequence, topology, protein concentration and formulation

700   diversity, will be needed to test this further in the future, with some datasets already emerging

701   to this aim,[49] providing the groundwork needed to test our general framework's broad

702   applicability.

Conclusion

Herein, we subjected nine different formulation:mAbs to an array of diverse lab- and computer-based developability assays, alongside rate of relative monomer loss at 5-, 25- and 40 ˚C to obtain a test dataset with which to develop a rational framework for DA selection. Through adopting a robust statistical approach, we demonstrate it is possible to identify a minimal set of DAs capable of predicting a specific critical quality attribute of the development pipeline. Combining these variables using the LASSO approach yields a quantifiable "Holistic Developability Parameter" (HDP) by which candidates can be ranked by user-determined measure of manufacturability irrespective of often conflicting results from multiple, separate DAs. Here we demonstrate the approach by using day zero DAs to predict the storage stability at 25 °C, since the latter is expensive (in terms of both time and material), yet essential within the regulatory framework. The streamlining of development in this way supports intensification within the drug pipeline, reducing costs and increasing sustainability.

Supporting Information

Further information on the developability assays, data distributions for each assay variable, raw data for the AS and EFD studies, as well as statistical analysis, are available in the Supporting Information.

The main analysed data, including the ranked data, are available *via* the University of Leeds repository (https://doi.org/10.5518/1470). Other data are available from the corresponding authors upon reasonable request.

Conflict of interest statement

I.T, J.C.S, K.D, N.B, P.W.A.D, C.L and N.J.D are all employees of AstraZeneca PLC. M.G.B was an employee of AstraZeneca PLC at the inception of the study. All other authors declare no conflicts of interest.

References

(1) Rathore, A. S. Quality by Design (QbD)-Based Process Development for Purification of a Biotherapeutic. *Trends Biotechnol* **2016**, *34* (5), 358–370. https://doi.org/10.1016/j.tibtech.2016.01.003.

(2) Svilenov, H. L.; Arosio, P.; Menzen, T.; Tessier, P.; Sormanni, P. Approaches to Expand the Conventional Toolbox for Discovery and Selection of Antibodies with Drug-like Physicochemical Properties. *MAbs* **2023**, *15* (1), 2164459. https://doi.org/10.1080/19420862.2022.2164459.

(3) Xu, Y.; Wang, D.; Mason, B.; Rossomando, T.; Li, N.; Liu, D.; Cheung, J. K.; Xu, W.; Raghava, S.; Katiyar, A.; Nowak, C.; Xiang, T.; Dong, D. D.; Sun, J.; Beck, A.; Liu, H. Structure, Heterogeneity and Developability Assessment of Therapeutic Antibodies. *MAbs* **2019**, *11* (2), 239–264. https://doi.org/10.1080/19420862.2018.1553476.

(4) Jain, T.; Sun, T.; Durand, S.; Hall, A.; Houston, N. R.; Nett, J. H.; Sharkey, B.; Bobrowicz, B.; Caffry, I.; Yu, Y.; Cao, Y.; Lynaugh, H.; Brown, M.; Baruah, H.; Gray, L. T.; Krauland, E. M.; Xu, Y.; Vásquez, M.; Wittrup, K. D. Biophysical Properties of the Clinical-Stage Antibody Landscape. *Proceedings of the National Academy of Sciences* **2017**, *114* (5), 944–949. https://doi.org/10.1073/pnas.1616408114.

(5) Sormanni, P.; Aprile, F. A.; Vendruscolo, M. The CamSol Method of Rational Design of Protein Mutants with Enhanced Solubility. *J Mol Biol* **2015**, *427* (2), 478–490. https://doi.org/10.1016/j.jmb.2014.09.026.

(6) Sormanni, P.; Amery, L.; Ekizoglou, S.; Vendruscolo, M.; Popovic, B. Rapid and Accurate in Silico Solubility Screening of a Monoclonal Antibody Library. *Sci Rep* **2017**, *7* (1), 8200. https://doi.org/10.1038/s41598-017-07800-w.

(7) Wolf Pérez, A. M.; Sormanni, P.; Andersen, J. S.; Sakhnini, L. I.; Rodriguez-Leon, I.; Bjelke, J. R.; Gajhede, A. J.; De Maria, L.; Otzen, D. E.; Vendruscolo, M.; Lorenzen, N. In Vitro and in Silico Assessment of the Developability of a Designed Monoclonal Antibody Library. *MAbs* **2019**, *11* (2), 388–400. https://doi.org/10.1080/19420862.2018.1556082.

(8) Raybould, M. I. J.; Marks, C.; Krawczyk, K.; Taddese, B.; Nowak, J.; Lewis, A. P.; Bujotzek, A.; Shi, J.; Deane, C. M. Five Computational Developability Guidelines for Therapeutic Antibody Profiling. *Proceedings of the National Academy of Sciences* **2019**, *116* (10), 4025–4030. https://doi.org/10.1073/pnas.1810576116.

(9) Blech, M.; Melien, R.; Tschammer, N.; Presser, B.; Hinderberger, D.; Garidel, P. Expanding the Toolbox for Predictive Parameters Describing Antibody Stability Considering Thermodynamic and Kinetic Determinants. *Pharm Res* **2021**, *38* (12), 2065–2089. https://doi.org/10.1007/s11095-021-03120-x.

(10) Trikeriotis, M.; Akbulatov, S.; Esposito, U.; Anastasiou, A.; Leszczyszyn, O. I. Analytical Workflows to Unlock Predictive Power in Biotherapeutic Developability. *Pharm Res* **2023**, *40* (2), 487–500. https://doi.org/10.1007/s11095-022-03448-y.

(11) Kohli, N.; Jain, N.; Geddie, M. L.; Razlog, M.; Xu, L.; Lugovskoy, A. A. A Novel Screening Method to Assess Developability of Antibody-like Molecules. *MAbs* **2015**, *7* (4), 752–758. https://doi.org/10.1080/19420862.2015.1048410.

786 (12) Kopp, M. R. G.; Wolf Pérez, A. M.; Zucca, M. V.; Capasso Palmiero, U.; Friedrichsen, B.;
787   Lorenzen, N.; Arosio, P. An Accelerated Surface-Mediated Stress Assay of Antibody Instability
788   for Developability Studies. *MAbs* **2020**, *12* (1), 1815995.
789   https://doi.org/10.1080/19420862.2020.1815995.

790 (13) Kopp, M. R. G.; Capasso Palmiero, U.; Arosio, P. A Nanoparticle-Based Assay To Evaluate
791   Surface-Induced Antibody Instability. *Mol Pharm* **2020**, *17* (3), 909–918.
792   https://doi.org/10.1021/acs.molpharmaceut.9b01168.

793 (14) Ebo, J. S.; Saunders, J. C.; Devine, P. W. A.; Gordon, A. M.; Warwick, A. S.; Schiffrin, B.; Chin, S.
794   E.; England, E.; Button, J. D.; Lloyd, C.; Bond, N. J.; Ashcroft, A. E.; Radford, S. E.; Lowe, D. C.;
795   Brockwell, D. J. An in Vivo Platform to Select and Evolve Aggregation-Resistant Proteins. *Nat*
796   *Commun* **2020**, *11* (1), 1816. https://doi.org/10.1038/s41467-020-15667-1.

797 (15) van der Kant, R.; Karow-Zwick, A. R.; Van Durme, J.; Blech, M.; Gallardo, R.; Seeliger, D.;
798   Aßfalg, K.; Baatsen, P.; Compernolle, G.; Gils, A.; Studts, J. M.; Schulz, P.; Garidel, P.;
799   Schymkowitz, J.; Rousseau, F. Prediction and Reduction of the Aggregation of Monoclonal
800   Antibodies. *J Mol Biol* **2017**, *429* (8), 1244–1261. https://doi.org/10.1016/j.jmb.2017.03.014.

801 (16) Willis, L. F.; Kumar, A.; Jain, T.; Caffry, I.; Xu, Y.; Radford, S. E.; Kapur, N.; Vásquez, M.;
802   Brockwell, D. J. The Uniqueness of Flow in Probing the Aggregation Behavior of Clinically
803   Relevant Antibodies. *Engineering Reports* **2020**, *2* (5), 1–13.
804   https://doi.org/10.1002/eng2.12147.

805 (17) Svilenov, H.; Winter, G. The ReFOLD Assay for Protein Formulation Studies and Prediction of
806   Protein Aggregation during Long-Term Storage. *European Journal of Pharmaceutics and*
807   *Biopharmaceutics* **2019**, *137* (February), 131–139.
808   https://doi.org/10.1016/j.ejpb.2019.02.018.

809 (18) Dobson, C. L.; Devine, P. W. A.; Phillips, J. J.; Higazi, D. R.; Lloyd, C.; Popovic, B.; Arnold, J.;
810   Buchanan, A.; Lewis, A.; Goodman, J.; van der Walle, C. F.; Thornton, P.; Vinall, L.; Lowne, D.;
811   Aagaard, A.; Olsson, L.-L.; Ridderstad Wollberg, A.; Welsh, F.; Karamanos, T. K.; Pashley, C. L.;
812   Iadanza, M. G.; Ranson, N. A.; Ashcroft, A. E.; Kippen, A. D.; Vaughan, T. J.; Radford, S. E.;
813   Lowe, D. C. Engineering the Surface Properties of a Human Monoclonal Antibody Prevents
814   Self-Association and Rapid Clearance in Vivo. *Sci Rep* **2016**, *6* (November), 38644.
815   https://doi.org/10.1038/srep38644.

816 (19) Gentiluomo, L.; Svilenov, H. L.; Augustijn, D.; El Bialy, I.; Greco, M. L.; Kulakova, A.;
817   Indrakumar, S.; Mahapatra, S.; Morales, M. M.; Pohl, C.; Roche, A.; Tosstorff, A.; Curtis, R.;
818   Derrick, J. P.; Nørgaard, A.; Khan, T. A.; Peters, G. H. J.; Pluen, A.; Rinnan, Å.; Streicher, W. W.;
819   van der Walle, C. F.; Uddin, S.; Winter, G.; Roessner, D.; Harris, P.; Frieß, W. Advancing
820   Therapeutic Protein Discovery and Development through Comprehensive Computational and
821   Biophysical Characterization. *Mol Pharm* **2020**, *17* (2), 426–440.
822   https://doi.org/10.1021/acs.molpharmaceut.9b00852.

823 (20) Bailly, M.; Mieczkowski, C.; Juan, V.; Metwally, E.; Tomazela, D.; Baker, J.; Uchida, M.;
824   Kofman, E.; Raoufi, F.; Motlagh, S.; Yu, Y.; Park, J.; Raghava, S.; Welsh, J.; Rauscher, M.;
825   Raghunathan, G.; Hsieh, M.; Chen, Y.-L.; Nguyen, H. T.; Nguyen, N.; Cipriano, D.; Fayadat-
826   Dilman, L. Predicting Antibody Developability Profiles Through Early Stage Discovery
827   Screening. *MAbs* **2020**, *12* (1). https://doi.org/10.1080/19420862.2020.1743053.

828 (21) Thiagarajan, G.; Semple, A.; James, J. K.; Cheung, J. K.; Shameem, M. A Comparison of
829   Biophysical Characterization Techniques in Predicting Monoclonal Antibody Stability. *MAbs*
830   **2016**, *8* (6), 1088–1097. https://doi.org/10.1080/19420862.2016.1189048.

831 (22) Narayanan, H.; Dingfelder, F.; Condado Morales, I.; Patel, B.; Heding, K. E.; Bjelke, J. R.;
832   Egebjerg, T.; Butté, A.; Sokolov, M.; Lorenzen, N.; Arosio, P. Design of Biopharmaceutical
833   Formulations Accelerated by Machine Learning. *Mol Pharm* **2021**, *18* (10), 3843–3853.
834   https://doi.org/10.1021/acs.molpharmaceut.1c00469.

835 (23) Kingsbury, J. S.; Saini, A.; Auclair, S. M.; Fu, L.; Lantz, M. M.; Halloran, K. T.; Calero-Rubio, C.;
836   Schwenger, W.; Airiau, C. Y.; Zhang, J.; Gokarn, Y. R. A Single Molecular Descriptor to Predict
837   Solution Behavior of Therapeutic Antibodies. *Sci Adv* **2020**, *6* (32), eabb0372.
838   https://doi.org/10.1126/sciadv.abb0372.

839 (24) ICH. *INTERNATIONAL CONFERENCE ON HARMONISATION OF TECHNICAL REQUIREMENTS FOR*
840   *REGISTRATION OF PHARMACEUTICALS FOR HUMAN USE ICH HARMONISED TRIPARTITE*
841   *GUIDELINE STABILITY TESTING OF NEW DRUG SUBSTANCES AND PRODUCTS Q1A(R2)*; 2003.

842 (25) Daramola, O.; Stevenson, J.; Dean, G.; Hatton, D.; Pettman, G.; Holmes, W.; Field, R. A High-
843   yielding CHO Transient System: Coexpression of Genes Encoding EBNA-1 and GS Enhances
844   Transient Protein Expression. *Biotechnol Prog* **2014**, *30* (1), 132–141.
845   https://doi.org/10.1002/btpr.1809.

846 (26) Dobson, J.; Kumar, A.; Willis, L. F.; Tuma, R.; Higazi, D. R.; Turner, R.; Lowe, D. C.; Ashcroft, A.
847   E.; Radford, S. E.; Kapur, N.; Brockwell, D. J. Inducing Protein Aggregation by Extensional Flow.
848   *Proceedings of the National Academy of Sciences* **2017**, *114* (18), 4673–4678.
849   https://doi.org/10.1073/pnas.1702724114.

850 (27) Willis, L. F.; Kumar, A.; Dobson, J.; Bond, N. J.; Lowe, D.; Turner, R.; Radford, S. E.; Kapur, N.;
851   Brockwell, D. J. Using Extensional Flow to Reveal Diverse Aggregation Landscapes for Three
852   IgG1 Molecules. *Biotechnol Bioeng* **2018**, *115* (5), 1216–1225.
853   https://doi.org/10.1002/bit.26543.

854 (28) Willis, L. F.; Toprani, V.; Wijetunge, S.; Sievers, A.; Lin, L.; Williams, J.; Crowley, T. J.; Radford,
855   S. E.; Kapur, N.; Brockwell, D. J. Exploring a Role for Flow-Induced Aggregation Assays in
856   Platform Formulation Optimisation for Antibody-Based Proteins. *J Pharm Sci* **2024**, *113* (3),
857   625–636. https://doi.org/10.1016/j.xphs.2023.10.031.

858 (29) Lu, Y.; Phillips, C. A.; Langston, M. A. A Robustness Metric for Biological Data Clustering
859   Algorithms. *BMC Bioinformatics* **2019**, *20* (S15), 503. https://doi.org/10.1186/s12859-019-
860   3089-6.

861 (30) Tibshirani, R. Regression Shrinkage and Selection via the Lasso. *Source: Journal of the Royal*
862   *Statistical Society. Series B (Methodological)* **1996**, *58* (1), 267–288.

863 (31) Strickley, R. G.; Lambert, W. J. A Review of Formulations of Commercially Available
864   Antibodies. *J Pharm Sci* **2021**, *110* (7), 2590-2608.e56.
865   https://doi.org/10.1016/j.xphs.2021.03.017.

866 (32) Hötzel, I.; Theil, F.-P.; Bernstein, L. J.; Prabhu, S.; Deng, R.; Quintana, L.; Lutman, J.; Sibia, R.;
867   Chan, P.; Bumbaca, D.; Fielder, P.; Carter, P. J.; Kelley, R. F. A Strategy for Risk Mitigation of
868   Antibodies with Fast Clearance. *MAbs* **2012**, *4* (6), 753–760.
869   https://doi.org/10.4161/mabs.22189.

870   (33)   Rathore, N.; Rajan, R. S. Current Perspectives on Stability of Protein Drug Products during
871   Formulation, Fill and Finish Operations. *Biotechnol Prog* **2008**, *24* (3), 504–514.
872   https://doi.org/10.1021/bp070462h.

873   (34)   Baek, Y.; Zydney, A. L. Intermolecular Interactions in Highly Concentrated Formulations of
874   Recombinant Therapeutic Proteins. *Curr Opin Biotechnol* **2018**, *53*, 59–64.
875   https://doi.org/10.1016/j.copbio.2017.12.016.

876   (35)   Mahler, H.-C.; Friess, W.; Grauschopf, U.; Kiese, S. Protein Aggregation: Pathways, Induction
877   Factors and Analysis. *J Pharm Sci* **2009**, *98* (9), 2909–2934.
878   https://doi.org/10.1002/jps.21566.

879   (36)   Wang, W.; Roberts, C. J. Non-Arrhenius Protein Aggregation. *AAPS J* **2013**, *15* (3), 840–851.
880   https://doi.org/10.1208/s12248-013-9485-3.

881   (37)   Wälchli, R.; Vermeire, P.-J.; Massant, J.; Arosio, P. Accelerated Aggregation Studies of
882   Monoclonal Antibodies: Considerations for Storage Stability. *J Pharm Sci* **2020**, *109* (1), 595–
883   602. https://doi.org/10.1016/j.xphs.2019.10.048.

884   (38)   Goldberg, D. S.; Lewus, R. A.; Esfandiary, R.; Farkas, D. C.; Mody, N.; Day, K. J.; Mallik, P.;
885   Tracka, M. B.; Sealey, S. K.; Samra, H. S. Utility of High Throuput Screening Techniques to
886   Predict Stability of Monoclonal Antibody Formulations During Early Stage Development. *J*
887   *Pharm Sci* **2017**, *106* (8), 1971–1977. https://doi.org/10.1016/j.xphs.2017.04.039.

888   (39)   Kuzman, D.; Bunc, M.; Ravnik, M.; Reiter, F.; Žagar, L.; Bončina, M. Long-Term Stability
889   Predictions of Therapeutic Monoclonal Antibodies in Solution Using Arrhenius-Based Kinetics.
890   *Sci Rep* **2021**, *11* (1), 20534. https://doi.org/10.1038/s41598-021-99875-9.

891   (40)   Bunc, M.; Hadži, S.; Graf, C.; Bončina, M.; Lah, J. Aggregation Time Machine: A Platform for
892   the Prediction and Optimization of Long-Term Antibody Stability Using Short-Term Kinetic
893   Analysis. *J Med Chem* **2022**, *65* (3), 2623–2632.
894   https://doi.org/10.1021/acs.jmedchem.1c02010.

895   (41)   Huelsmeyer, M.; Kuzman, D.; Bončina, M.; Martinez, J.; Steinbrugger, C.; Weusten, J.; Calero-
896   Rubio, C.; Roche, W.; Niederhaus, B.; VanHaelst, Y.; Hrynyk, M.; Ballesta, P.; Achard, H.;
897   Augusto, S.; Guillois, M.; Pszczolinski, C.; Gerasimov, M.; Neyra, C.; Ponduri, D.; Ramesh, S.;
898   Clénet, D. A Universal Tool for Stability Predictions of Biotherapeutics, Vaccines and in Vitro
899   Diagnostic Products. *Sci Rep* **2023**, *13* (1), 10077. https://doi.org/10.1038/s41598-023-35870-
900   6.

901   (42)   Wang, W.; Roberts, C. J. Protein Aggregation – Mechanisms, Detection, and Control. *Int J*
902   *Pharm* **2018**, *550* (1–2), 251–268. https://doi.org/10.1016/j.ijpharm.2018.08.043.

903   (43)   Chakroun, N.; Hilton, D.; Ahmad, S. S.; Platt, G. W.; Dalby, P. A. Mapping the Aggregation
904   Kinetics of a Therapeutic Antibody Fragment. *Mol Pharm* **2016**, *13* (2), 307–319.
905   https://doi.org/10.1021/acs.molpharmaceut.5b00387.

906   (44)   Ausserwöger, H.; Schneider, M. M.; Herling, T. W.; Arosio, P.; Invernizzi, G.; Knowles, T. P. J.;
907   Lorenzen, N. Non-Specificity as the Sticky Problem in Therapeutic Antibody Development. *Nat*
908   *Rev Chem* **2022**, *6* (12), 844–861. https://doi.org/10.1038/s41570-022-00438-x.

909   (45)   Porebski, B. T.; Balmforth, M.; Browne, G.; Riley, A.; Jamali, K.; Fürst, M. J. L. J.; Velic, M.;
910   Buchanan, A.; Minter, R.; Vaughan, T.; Holliger, P. Rapid Discovery of High-Affinity Antibodies

911   via Massively Parallel Sequencing, Ribosome Display and Affinity Screening. *Nat Biomed Eng*
912   **2023**, *8* (3), 214–232. https://doi.org/10.1038/s41551-023-01093-3.

913   (46)   Makowski, E. K.; Wang, T.; Zupancic, J. M.; Huang, J.; Wu, L.; Schardt, J. S.; De Groot, A. S.;
914   Elkins, S. L.; Martin, W. D.; Tessier, P. M. Optimization of Therapeutic Antibodies for Reduced
915   Self-Association and Non-Specific Binding via Interpretable Machine Learning. *Nat Biomed*
916   *Eng* **2024**, *8* (1), 45–56. https://doi.org/10.1038/s41551-023-01074-6.

917   (47)   Jain, T.; Boland, T.; Vásquez, M. Identifying Developability Risks for Clinical Progression of
918   Antibodies Using High-Throughput in Vitro and in Silico Approaches. *MAbs* **2023**, *15* (1),
919   2200540. https://doi.org/10.1080/19420862.2023.2200540.

920   (48)   Willis, L. F.; Kumar, A.; Jain, T.; Caffry, I.; Xu, Y.; Radford, S. E.; Kapur, N.; Vásquez, M.;
921   Brockwell, D. J. The Uniqueness of Flow in Probing the Aggregation Behavior of Clinically
922   Relevant Antibodies. *Engineering Reports* **2020**, *2* (5). https://doi.org/10.1002/eng2.12147.

923   (49)   Condado-Morales, I.; Dingfelder, F.; Waibel, I.; Turnbull, O. M.; Patel, B.; Cao, Z.; Rose Bjelke,
924   J.; Nedergaard Grell, S.; Bennet, A.; Hummer, A. M.; Raybould, M. I. J.; Deane, C. M.; Egebjerg,
925   T.; Lorenzen, N.; Arosio, P. A Comparative Study of the Developability of Full-Length
926   Antibodies, Fragments, and Bispecific Formats Reveals Higher Stability Risks for Engineered
927   Constructs. *MAbs* **2024**, *16* (1). https://doi.org/10.1080/19420862.2024.2403156.

928   (50)   Brader, M. L.; Estey, T.; Bai, S.; Alston, R. W.; Lucas, K. K.; Lantz, S.; Landsman, P.; Maloney, K.
929   M. Examination of Thermal Unfolding and Aggregation Profiles of a Series of Developable
930   Therapeutic Monoclonal Antibodies. *Mol Pharm* **2015**, *12* (4), 1005–1017.
931   https://doi.org/10.1021/mp400666b.

932   (51)   Armstrong, G. B.; Shah, V.; Sanches, P.; Patel, M.; Casey, R.; Jamieson, C.; Burley, G. A.; Lewis,
933   W.; Rattray, Z. A Framework for the Biophysical Screening of Antibody Mutations Targeting
934   Solvent-Accessible Hydrophobic and Electrostatic Patches for Enhanced Viscosity Profiles.
935   *Comput Struct Biotechnol J* **2024**, *23*, 2345–2357. https://doi.org/10.1016/j.csbj.2024.05.041.

936   (52)   Spearman, C. The Proof and Measurement of Association between Two Things. *Source: The*
937   *American Journal of Psychology , Autumn-Winter* **1904**, *100* (4), 72–101.

938   (53)   Starr, C. G.; Makowski, E. K.; Wu, L.; Berg, B.; Kingsbury, J. S.; Gokarn, Y. R.; Tessier, P. M.
939   Ultradilute Measurements of Self-Association for the Identification of Antibodies with
940   Favorable High-Concentration Solution Properties. *Mol Pharm* **2021**, *18* (7), 2744–2753.
941   https://doi.org/10.1021/acs.molpharmaceut.1c00280.

942   (54)   Melchore, J. A. Sound Practices for Consistent Human Visual Inspection. *AAPS PharmSciTech*
943   **2011**, *12* (1), 215–212. https://doi.org/10.1208/s12249-010-9577-7.

944   (55)   Murphy, M. I.; Bruque, M.; Hanford, A.; Trayton, I.; Handali, M.; Leissa, J. A.; Hasige, S.; Day,
945   K.; Patel, S. M. Qualitative High-Throughput Analysis of Subvisible Particles in Biological
946   Formulations Using Backgrounded Membrane Imaging. *J Pharm Sci* **2022**, *111* (6), 1605–1613.
947   https://doi.org/10.1016/j.xphs.2022.03.010.

948   (56)   Dai, L.; Davis, J.; Nagapudi, K.; Mantik, P.; Zhang, K.; Pellett, J. D.; Wei, B. Predicting Long-
949   Term Stability of an Oral Delivered Antibody Drug Product with Accelerated Stability
950   Assessment Program Modeling. *Mol Pharm* **2024**, *21* (1), 325–332.
951   https://doi.org/10.1021/acs.molpharmaceut.3c00877.

952 (57) Dillon, M.; Xu, J.; Thiagarajan, G.; Skomski, D.; Procopio, A. Predicting the Long-Term Stability
953   of Biologics with Short-Term Data. *Mol Pharm* **2024**, *21* (9), 4673–4687.
954   https://doi.org/10.1021/acs.molpharmaceut.4c00609.

955 (58) Bashour, H.; Smorodina, E.; Pariset, M.; Zhong, J.; Akbar, R.; Chernigovskaya, M.; Lê Quý, K.;
956   Snapkow, I.; Rawat, P.; Krawczyk, K.; Sandve, G. K.; Gutierrez-Marcos, J.; Gutierrez, D. N.-Z.;
957   Andersen, J. T.; Greiff, V. Biophysical Cartography of the Native and Human-Engineered
958   Antibody Landscapes Quantifies the Plasticity of Antibody Developability. *Commun Biol* **2024**,
959   *7* (1), 922. https://doi.org/10.1038/s42003-024-06561-3.

960 (59) Satława, T.; Tarkowski, M.; Wróbel, S.; Dudzic, P.; Gawłowski, T.; Klaus, T.; Orłowski, M.;
961   Kostyn, A.; Kumar, S.; Buchanan, A.; Krawczyk, K. LAP: Liability Antibody Profiler by Sequence
962   & Structural Mapping of Natural and Therapeutic Antibodies. *PLoS Comput Biol* **2024**, *20* (3).
963   https://doi.org/10.1371/journal.pcbi.1011881.

964